Langmuir

ARTICLE

pubs.acs.org/Langmuir

Nanoparticle Dispersion and Aggregation in Polymer Nanocomposites: Insights from Molecular Dynamics Simulation

Jun Liu,[†,‡] Yangyang Gao,[†] Dapeng Cao,[*,†,‡] Liqun Zhang,[*,†] and Zhanhu Guo[*,§]

[†]Key Laboratory of Beijing City on Preparation and Processing of Novel Polymer Materials and [‡]Division of Molecular and Materials Simulation, State Key Laboratory of Organic−Inorganic Composites, Beijing University of Chemical Technology, Beijing 100029, People's Republic of China

[§]Integrated Composites Laboratory (ICL), Dan F. Smith Department of Chemical Engineering, Lamar University, Beaumont, Texas 77710, United States

ABSTRACT: It is a great challenge to fully understand the microscopic dispersion and aggregation of nanoparticles (NPs) in polymer nanocomposites (PNCs) through experimental techniques. Here, coarse-grained molecular dynamics is adopted to study the dispersion and aggregation mechanisms of spherical NPs in polymer melts. By tuning the polymer−filler interaction in a wide range at both low and high filler loadings, we qualitatively sketch the phase behavior of the PNCs and structural spatial organization of the fillers mediated by the polymers, which emphasize that a homogeneous filler dispersion exists just at the intermediate interfacial interaction, in contrast with traditional viewpoints. The conclusion is in good agreement with the theoretically predicted results from Schweizer et al. Besides, to mimick the experimental coarsening process of NPs in polymer matrixes (*ACS Nano* **2008**, *2*, 1305), by grafting polymer chains on the filler surface, we obtain a good filler dispersion with a large interparticle distance. Considering the PNC system without the presence of chemical bonding between the NPs and the grafted polymer chains, the resulting good dispersion state is further used to investigate the effects of the temperature, polymer−filler interaction, and filler size on the filler aggregation process. It is found that the coarsening or aggregation process of the NPs is sensitive to the temperature, and the aggregation extent reaches the minimum in the case of moderate polymer−filler interaction, because in this case a good dispersion is obtained. That is to say, once the filler achieves a good dispersion in a polymer matrix, the properties of the PNCs will be improved significantly, because the coarsening process of the NPs will be delayed and the aging of the PNCs will be slowed.

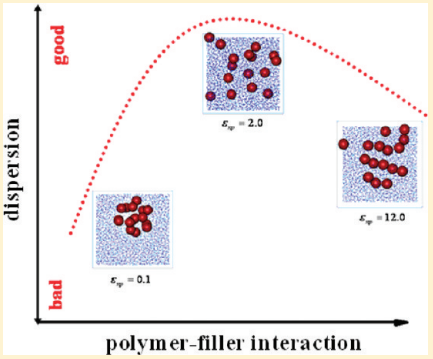

1. INTRODUCTION

Polymer nanocomposites (PNCs), by dispersing organic or inorganic nanoparticles (NPs) such as spheres, rods, and plates in polymer matrixes, have attracted considerable academic and industrial attention. PNCs always possess greatly enhanced mechanical, optical, electrical, and flame retardancy properties and so on.[1] However, one main impediment in the development of high-performance PNCs is to realize a good dispersion of NPs, owing to the strong interparticle interactions and weak polymer−nanoparticle interfacial interaction. To address this issue, various experimental, theoretical, and simulation studies have been performed. For instance, Mackay et al.[2,3] found that a thermodynamically stable dispersion of NPs in a polymer matrix can be enhanced only when the radius of gyration of the linear polymer chain is greater than the radius of the nanoparticle, however, which can be obtained only with the correct processing strategy. Similarly, in the case of cross-linked polystyrene (PS) NPs mixed with linear PS chains, the key role of entropy in the nanoparticle dispersion is indentified.[4] Meanwhile, Krishnamoorti[5] has reviewed various experimental methods to quantitatively characterize the nanoparticle dispersion, such as atomic force microscopy (AFM), transmission electron microscopy (TEM), and scattering, electrical, and mechanical spectroscopy. By considering the qualitative TEM images as the "gold standard" for dispersion characterization, Khare et al.[6] have also developed a free-space length method to quantitatively analyze the dispersion of NPs.

Recently, by using the microscopic polymer reference interaction site model (PRISM), Schweizer et al.[7] found that, for hard-sphere fillers, four general categories of polymer-mediated nanoparticle organization exist: (i) contact aggregation, (ii) segmental-level tight particle bridging, (iii) steric stabilization due to thermodynamically stable "bound polymer layers", and (iv) "telebridging". Furthermore, they also obtained three dispersion phase diagrams for hard fillers: (i) macroscopic phase separation at low polymer−filler interaction, (ii) enthalpically stabilized miscible fluid at moderate interfacial interaction, and (iii) microscopic phase separation through local bridging of the fillers by polymer chains. Very recently, Ganesan et al.[8] reviewed advances of the equilibrium dispersion and structure of PNCs on the basis of

Received: March 22, 2011
Revised: May 6, 2011
Published: May 19, 2011

dx.doi.org/10.1021/la201073m | *Langmuir* 2011, 27, 7926–7933

the mean-field models, including NP and grafted NP dispersion in homopolymers and the self-assembly and organization of the NPs in block copolymers. Meanwhile, the development of microscopic predictive theories to correlate the equilibrium structure, polymer-mediated interactions, and phase behavior of the PNCs has also been reviewed briefly on the basis of the liquid-state integral equation, density functional theory, and self-consistent mean field approaches.[9] Through molecular dynamics simulation, Starr et al.[10] have also explored several parameters influencing nanoparticle clustering. Fermeglia et al.[11] introduced multiscale molecular modeling to explore the dispersion of the NPs in the polymers.

It is known that one approach to disperse the NPs in the polymer matrixes is to functionalize the surface of the NPs with the same composition of the polymer chains as the polymer matrix. Experimental results indicate that the longer grafted polymer chains relative to the matrix chains are essential for dispersing the NPs.[12−14] Meanwhile, through the mean-field theory, Kumar et al.[15] found that the miscibility of the homopolymer-grafted NPs with the homopolymer matrixes is improved with decreasing particle radius and increasing brush chain length. Xu et al.[16] also employed the self-consistent field theory to examine the effects of the grafting density and the particle size on the interaction of brush-coated spheres immersed in a polymer melt. However, recent simulation results from Smith et al.[17] indicate that a good dispersion can be obtained as well by grafting shorter chains than the polymer matrix with relatively sparse grafting. Through the PRISM, Schweizer et al.[18−20] also discussed the structure and phase behavior of the lightly and moderately tethered NPs in polymer melts. Very recently, the interaction between copolymer-grafted NPs dispersed in homopolymers was also studied.[21]

Besides the investigation of nanoparticle dispersion, aggregation and flocculation of NPs are also very significant, which always take place in carbon black- or silica-filled rubber systems during the early stages of vulcanization when no dense rubber network has been formed yet.[22−26] For example, it is claimed that the filler network does not exist after the elastomer compounds are mixed, but forms in the process of storage through flocculation, particularly at higher temperatures, to which rubber compounds are exposed during shaping and vulcanization.[27] In addition, through coarse-grained molecular dynamics simulation, Kalra et al.[28] have recently probed how shear flow affects the kinetics of particle flocculation and found that shear significantly slows filler aggregation. Filippone et al.[29] experimentally investigated the influence of the clustering of fumed silica NPs in a polystyrene matrix on the linear viscoelasticity of the composite, which is dominated by the independent responses of the polymer melt and the filler network above a critical filler volume fraction. Definitely, in experiments during thermal annealing, particle coarsening in the polymer matrixes always occurs, which will influence the particle properties.[30,31] Green et al.[32] have studied ligand-stabilized gold NPs in poly(methyl methacrylate) (PMMA) thin films, finding that the nanoparticle growth process is well-described by the classical coarsening mechanisms. In fact, the coarsening and structural evolution of the NPs in polymer matrixes is closely related to their aggregation mechanism, and understanding the governing parameters that determine the time-dependent aggregation process will be of significant relevance to the further development and study of PNCs.

From the fundamental point of view, the filler dispersion and aggregation states are closely related to its size, shape, volume fraction, and filler−filler and polymer−filler interactions. In this work, we explore the mechanisms of the dispersion and aggregation of the NPs with different loading levels in the polymer matrixes by tuning the polymer−filler interaction in a wide range. Different from the work of Kalra et al.,[28] here we mainly focus on studying the aggregation mechanism under static conditions without the external shear force, which is also intended to mimick the coarsening process of the NPs in the polymer matrixes.[30,32] Meanwhile, our simulated results of the nanoparticle dispersion are also compared with the theoretical results from Schweizer et al.[7,33]

2. MODELS AND SIMULATION METHODS

In the simulation, the idealized model elastomer consists of 30 beads with a diameter equal to σ. The total number of simulated polymer monomers is 6000. The NPs are modeled as Lennard-Jones (LJ) spheres of radius R_n, which is equal to 2σ. In the simulation we set the mass of the polymer bead to be m, and since the radius of the nanoparticle is 4 times that of a bead, its mass is 64 times that of the bead. Similar to the literature,[34,35] here we use the modified LJ interaction to model the polymer−polymer, polymer−nanoparticle, and nanoparticle−nanoparticle interactions, as follows:

$$U_{ij}(r) = \begin{cases} 4\varepsilon_{ij}\left[\left(\frac{\sigma}{r-r_{EV}}\right)^{12} - \left(\frac{\sigma}{r-r_{EV}}\right)^{6}\right] - U(r_{cutoff}), & 0 < r - r_{EV} < r_{cutoff} \\ 0, & r - r_{EV} \geq r_{cutoff} \end{cases} \quad (1)$$

where r_{cutoff} stands for the distance $(r - r_{EV})$ at which the interaction is truncated and shifted so that the energy and force are zero. Here we offset the interaction range by r_{EV} to account for the excluded volume effects of different interaction sites. For polymer−nanoparticle and nanoparticle−nanoparticle interactions, r_{EV} is $R_n - \sigma/2$ and $2R_n - \sigma$, respectively, and for polymer−polymer interaction, r_{EV} becomes zero. The polymer−polymer interaction parameter and its cutoff distance are $\varepsilon_{pp} = 1.0$ and $r_{cutoff} = 2 \times 2^{1/6}$, and the nanoparticle−nanoparticle interaction parameter and its cutoff distance are $\varepsilon_{nn} = 1.0$ and $r_{cutoff} = 2^{1/6}$, while the nanoparticle−polymer interaction strength ε_{np} is changed to simulate different interfacial interactions with its cutoff distance $r_{cutoff} = 2.5$.

The interaction between the adjacent bonded monomers is represented by a stiff finite extensible nonlinear elastic (FENE) potential:

$$V_{FENE} = -0.5kR_0^2 \ln\left[1 - \left(\frac{r}{R_0}\right)^2\right] \quad (2)$$

where $k = 30(\varepsilon/\sigma^2)$ and $R_0 = 1.5\sigma$, guaranteeing a certain stiffness of the bonds while avoiding high-frequency modes and chain crossing.

Since it is not our aim to study a specific polymer, we use the LJ units where ε and σ are set to unity. This means that all calculated quantities are dimensionless. Similar to our recently published work,[34] we use the same method to initially construct the large system, and then the normal pressure and temperature (NPT) ensemble is adopted, where the temperature and pressure are fixed at $T^* = 1.0$ and $P^* = 0$, respectively, by using the Nose−Hoover temperature thermostat and pressure barostat. During the simulation, periodic boundary conditions are employed in all three directions. The velocity-Verlet[36] algorithm is used to integrate the equations of motion, with a time step $\delta t = 0.001$, where the time is reduced by the LJ time (τ).

Such structures are further equilibrated under the NPT ensemble with $T^* = 1.0$ and $P^* = 0$; the selection of the pressure follows the work of Smith,[35] which yields an equilibrium density greater than 0.7, corresponding to its

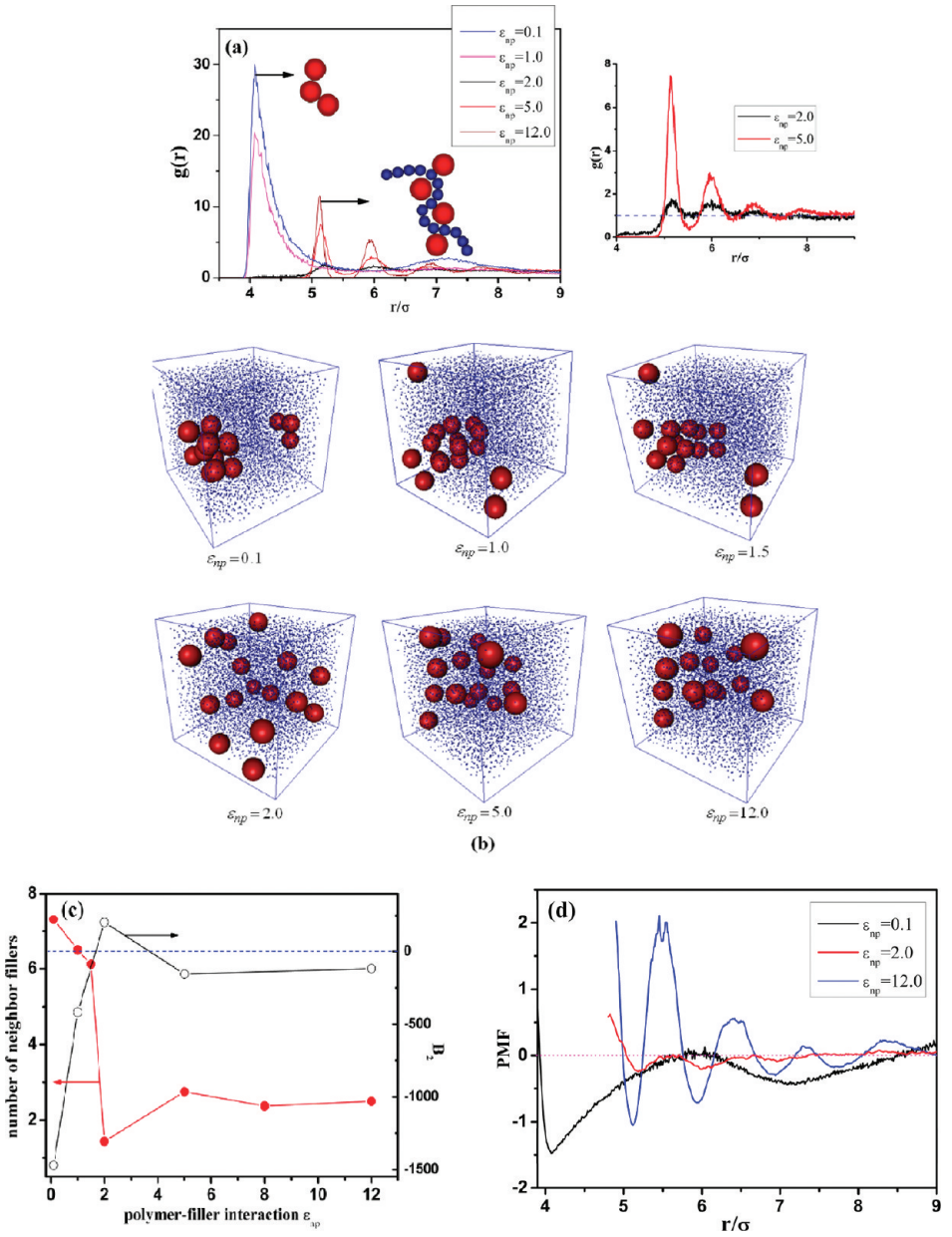

Figure 1. (a) RDF of NPs for different polymer−filler interactions ε_{np}. (b) Snapshots corresponding to different polymer−filler interactions. The red spheres denote the NPs, and for clarity the polymer chains are represented by blue points. (c) The left axis denotes the average number of neighbor fillers per filler as a function of the polymer−filler interaction, while the right axis represents the second virial coefficient with respect to the polymer−filler interaction. Note that the filler volume fraction is approximately 7.28%, and the filler size is $D = 4\sigma$. (d) PMF of filler particles at three typical polymer−filler interactions.

bulk state. The equilibrium length of the simulation box is approximately 20σ, except for the case of high filler volume fraction ($\phi = 24\%$). Similar to the equilibrium criterion in the literature,[37] we equilibrate all structures over a long time so that each chain has moved at least $2R_g$; the total equilibration time is accordingly increased for the larger systems. In addition, the equilibrated states at lower temperatures are obtained by cooling the state at higher temperatures. Such equilibrated structures are then used as starting structures for production runs of structural and dynamical analysis. All MD runs are carried out by using the large-scale atomic/molecular massively parallel simulator (LAMMPS), which was developed by Sandia National Laboratories.[38] More detailed simulation processes can be found in our previous papers.[34,39]

3. RESULTS AND DISCUSSION

3.1. Dispersion of NPs in the Polymer Matrix. To explore the dispersion and spatial distribution of the bare NPs in the polymer melts, we change the polymer−filler interaction from $\varepsilon_{np} = 0.1$ to $\varepsilon_{np} = 12.0$ while keeping the other parameters unchanged. First, we simulate the case in which the number of fillers equals 16, corresponding to a filler volume fraction of approximately $\phi = 7.28\%$. We use the radial distribution function (RDF) to characterize the filler dispersion state, as shown in Figure 1a. At a low polymer−filler interaction such as $\varepsilon_{np} = 0.1$ and 1.0, a peak appears at $r = 4\sigma$, indicating direct contact aggregation of the fillers. With an increase of the polymer−filler

dx.doi.org/10.1021/la201073m |*Langmuir* 2011, 27, 7926–7933

interaction, the NPs tend to form aggregates sandwiched by one or two polymer layers, which is reflected by the peaks located at $r = 5\sigma$ and 6σ, as schematically shown in Figure 1a. Particularly, for $\varepsilon_{np} = 2.0$, only small peaks appear without direct contact aggregation of the fillers, as shown in the right panel of Figure 1a. This observation implies that a good dispersion can be obtained at a moderate polymer−filler interaction. This simulated result is actually similar to the theoretical prediction.[33] Meanwhile, snapshots corresponding to the different polymer−filler interactions are also shown in Figure 1b. Obviously, a relatively good dispersion is seen for $\varepsilon_{np} = 2.0$.

To quantitatively characterize the filler dispersion state as a function of the polymer−filler interaction, the average number of NPs around every nanoparticle is calculated within a distance of $L = 6.5\sigma$, which includes all peaks shown in Figure 1a. The second virial coefficient B_2 of the NPs is also calculated, which is a good indicator of the tendency of NPs to aggregate or disperse,[35] given by

$$B_2 = -\frac{1}{2}\int_0^\infty [\exp(g(r) - 1)]4\pi r^2 \, dr \qquad (3)$$

where $g(r)$ is the RDF of the NPs shown in Figure 1a. A positive B_2 represents good dispersion of NPs, while a negative B_2 is an indicator of phase separation of the polymer and NPs. As shown in Figure 1c, the average number of fillers exhibits a minimum at $\varepsilon_{np} = 2.0$, supporting the conclusion that the best dispersion can be obtained only at a moderate polymer−filler interaction. The nonmonotonic change of the B_2 value also reflects the same dispersion behavior of the fillers, namely, from the direct contact aggregation, good dispersion to local bridging of the fillers by polymer chains. Meanwhile, the potential of mean force (PMF) of the NPs is also shown in Figure 1d. The results are obtained from the standard expression of the PMF related to $g(r)$:[40] $W_{nn}(r) = -k_B T \ln(g_{nn}(r))$, where k_B is the Boltzmann constant and $g_{nn}(r)$ is the RDF between the NPs. It can be seen in Figure 1d that, as ε_{np} increases, the PMF shows a more pronounced oscillation tendency, generating pockets of local potential for the NPs. For instance, at $\varepsilon_{np} = 0.1$, the PMF shows a global minimum at a distance $r = 4\sigma$, indicating its direct aggregation, while from $\varepsilon_{np} = 2.0$ to $\varepsilon_{np} = 12.0$, the local minimum at distances such as $r = 5\sigma$ and 6σ becomes more obvious, indicating an aggregation of the NPs via one and two monomer layers.

To further validate the conclusion that a moderate polymer−filler interaction results in good dispersion, the filler aggregation extent is monitored from the same initial state with a filler volume fraction $\phi = 7.28\%$ at three typical polymer−filler interactions, such as $\varepsilon_{np} = 0.1$, $\varepsilon_{np} = 2.0$, and $\varepsilon_{np} = 12.0$, as shown in Figure 2. Direct observation indicates that, at moderate interaction ($\varepsilon_{np} = 2.0$), the filler particles exhibit the best dispersion as a function of the time evolution, as evidenced clearly from the orthographic snapshots. To quantitatively characterize the filler aggregation extent, the average number of neighbor fillers per filler as a function of the time evolution is calculated and displayed in Figure 3, which also validates a relatively good dispersion state occurred at the moderate polymer−filler interaction. It is noted that the process driven by the thermal motions of NPs is to reach the thermodynamic equilibrium states of different polymer−filler interactions. Furthermore, it also illustrates that, at a strong polymer−filler interaction ($\varepsilon_{np} = 12.0$), the filler aggregation has reached its equilibrium. According to the results shown in

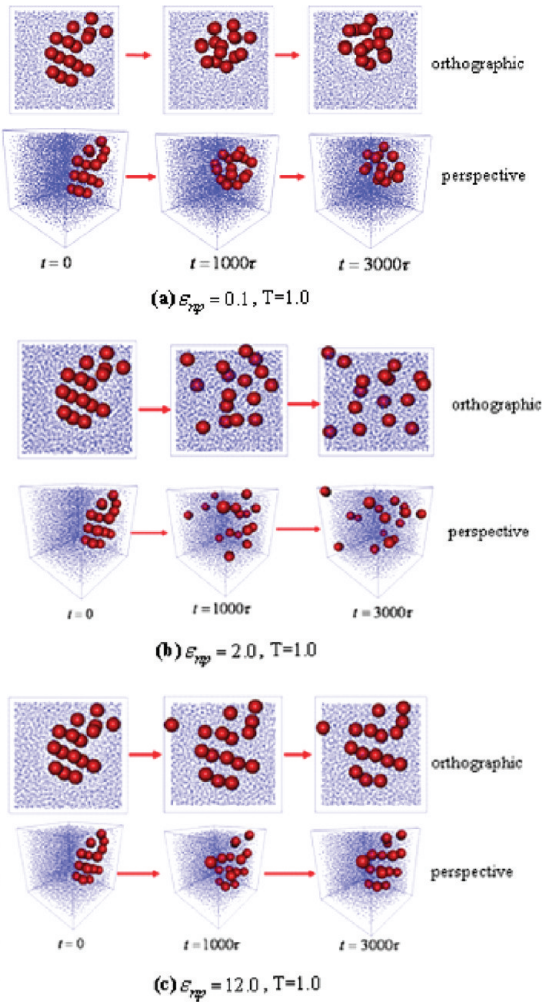

Figure 2. Snapshot for the aggregation process of fillers at three different polymer−filler interactions [(a) $\varepsilon_{np} = 0.1$, (b) $\varepsilon_{np} = 2.0$, and (c) $\varepsilon_{np} = 12.0$] at three times, such as $t = 0$, 1000τ, and 3000τ. The filler volume fraction is approximately 7.28%. Note that for better presentation the snapshots are shown from the orthographic and perspective aspect. The red spheres denote the NPs, and for clarity the polymer chains are represented by blue points. Note that the simulation temperature is set to $T = 1.0$.

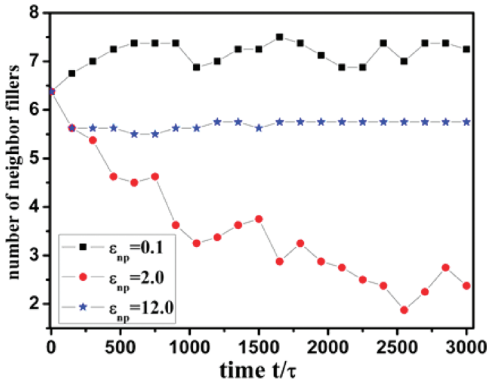

Figure 3. Average number of neighbor fillers per filler as a function of the time evolution from the same initial state.

Figures 1b and 3, the dispersion state changing with the polymer−filler interaction can be roughly sketched in Figure 4; three

dx.doi.org/10.1021/la201073m |*Langmuir* 2011, 27, 7926–7933

orthographic snapshots corresponding to ε_{np} = 0.1, 2.0, and 12.0 are also added to the figure.

A high filler volume fraction (ϕ = 24%) is as well simulated with a similarly varied polymer−filler interaction to probe the nanoparticle dispersion state. The simulated results are shown in Figure 5. Obviously, similar results are observed. However, in such a high filler loading, the interparticle distance is very small, and the dispersion state cannot be clearly reflected in the snapshots in Figure 5b. However, the change of the average number of neighbor particles suggests that a relatively good dispersion state can be obtained at a moderate polymer−filler interaction.

On the basis of the above simulated results, it is concluded that, at a low interfacial interaction, macroscopic phase separation between the NPs and the polymer chains exists, and with an increase of the polymer−filler interaction, the fillers will disperse into the polymer matrix uniformly, while at high interfacial interaction, a single polymer chain tends to adsorb several NPs at the same time. Correspondingly, the filler spatial organization as a function of the polymer−filler interaction shows three states: (i) phase separation of the filler and polymer, (ii) homogeneous dispersion of the filler, and (iii) local bridging of the filler via the polymer chains, as shown in Figure 6a. Obviously, the transition from state i to state ii results from the interfacial enthalpy gain. To analyze the transition from state ii to state iii, the equilibrium system with ε_{np} = 2.0 is chosen where the nanoparticle locations are fixed, and then the polymer−filler interaction is changed to ε_{np} = 5.0. After enough re-equilibrium, the NPs are allowed to move, and meanwhile the system enthalpy is monitored and is shown in Figure 6b. From the good dispersion to the local bridging of the fillers by polymer chains, the system enthalpy remains almost unchanged, indicating that the process is entropy dominated rather than enthalpy dominated. Namely, the single polymer chain tends to adsorb several NPs to avoid too much loss of the total chain entropy. It is noted that different from state i of direct aggregation of the NPs, the local aggregation of the NPs is bridged through polymer chains, attributed to a strong interaction between the polymer chains and NPs. In general, our analysis indicates that the transition process from state ii to state iii is entropy dominated, while the transition final state (namely state iii) is enthalpy dominated.

In addition, the aggregation process from the equilibrium dispersion state of ε_{np} = 2.0 to that of ε_{np} = 0.1 is monitored at different temperatures. The total number of neighbor fillers corresponding to the aggregation time $t = 1000\tau$ vs the temperature is shown in Figure 7. Obviously, an abrupt change is observed at approximately T = 0.5, corresponding to the glass transition. For glassy polymer matrixes below T_g, the nanoparticle aggregation rate becomes very slow, which indicates that the method of rapid cooling can obtain glassy PNCs with good nanoparticle dispersion.

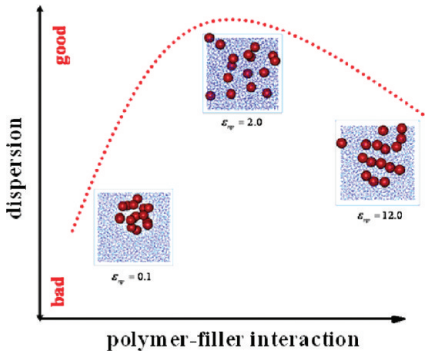

Figure 4. Change of the tendency of the filler dispersion state as a function of the polymer−filler interaction.

3.2. Coarsening Process of NPs in the Polymer Matrix. To mimick the experimental coarsening process of NPs in polymer

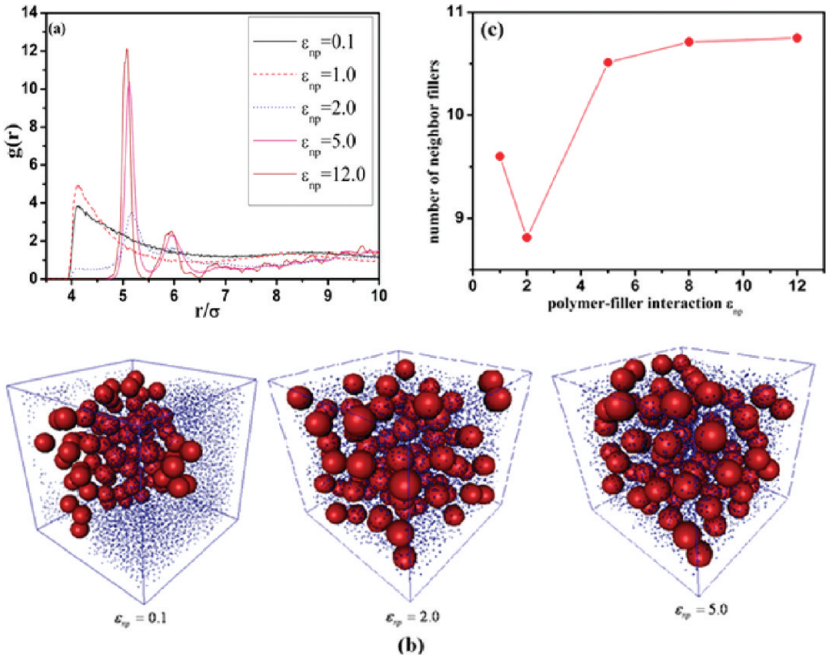

Figure 5. (a) RDF of the NPs for different polymer−filler interactions ε_{np}. (b) Snapshots corresponding to different polymer−filler interactions. The red spheres denote the NPs, and for clarity the polymer chains are represented by green points. (c) Average number of neighbor fillers as a function of the polymer−filler interaction. Note that the filler volume fraction is approximately 24%.

dx.doi.org/10.1021/la201073m |*Langmuir* 2011, 27, 7926–7933

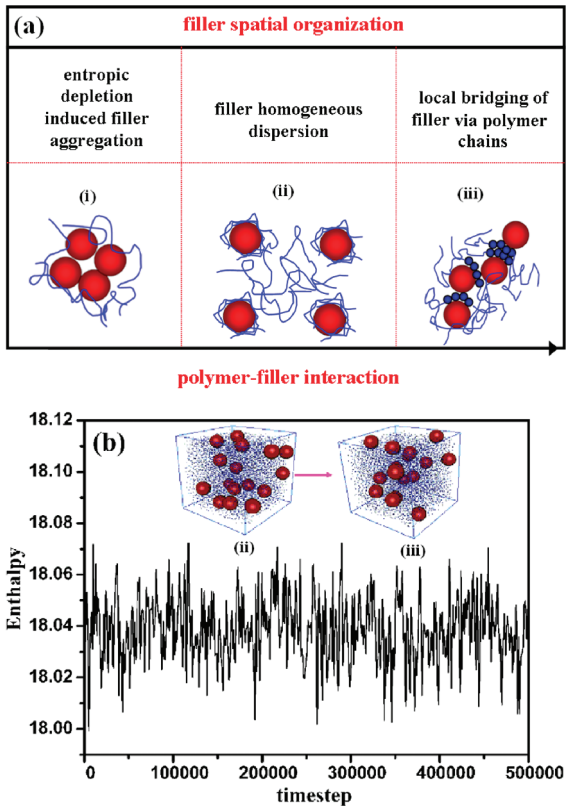

Figure 6. (a) Filler spatial organization as a function of the polymer−filler interaction. (b) The change of the system enthalpy is monitored during the aggregation process from polymer−filler interaction ε_{np} = 2.0 to ε_{np} = 5.0.

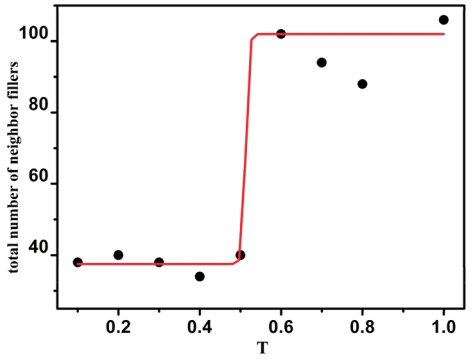

Figure 7. Total number of neighbor fillers corresponding to the aggregation time $t = 1000\tau$ with respect to the temperature.

matrixes,[32] the nanoparticle is grafted to the polymer chains with 10 beads following the approach used by Smith et al.[17] The number of grafted polymer chains per filler is 30, and the number of fillers is 10 with a diameter $D = 5\sigma$, resulting in a grafting density of 0.4. The polymer matrix chain also contains 10 beads. The snapshot of the grafted polymers on the 10 NPs is shown in Figure 8a. Note that the filler−filler interaction is attractive with its cutoff distance $r_{cutoff} = 2.5\sigma$, and the polymer−filler interaction is set to $\varepsilon_{np} = 1.0$. Similarly, RDF is used to characterize the filler dispersion state, as shown in Figure 8b, in which there is only a very small peak located at $r = 5\sigma$, indicating that there exists no direct contact aggregation of the NPs. Moreover, an

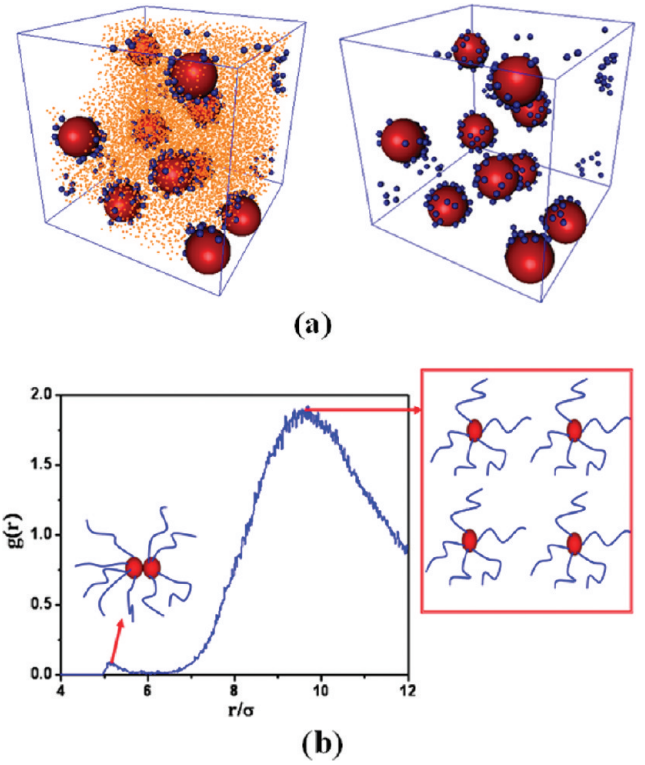

Figure 8. (a) Distribution of the grafted monomers on the nanoparticle. (b) RDF of grafted NPs. Here the filler size is set to be $D = 5\sigma$. Note that for clarity only the end monomers of the grafted chains are shown.

obvious peak occurs at around $r = 9.5\sigma$, which is attributed to the repulsion of the polymer chains grafted on the surface of the NPs. Through this grafting technique, a good dispersion of the NPs in the polymer matrix is obtained.

Since in practical PNCs the NPs are always dispersed in a thermodynamically nonequilibrium state, the coarsening and aggregation of the fillers will deteriorate the properties of the PNCs during their usage. Meanwhile, Green et al.[32] pointed out that the amount of theoretical work on the structural evolution of NPs in polymer matrixes is fairly small. Consequently, here the main concern is focused on the coarsening and aggregation process of the fillers. To explore the determinative parameters influencing the filler aggregation, all chemical bondings between the grafted points and the NPs are cut off and the cut polymer chains still remain in the system. Furthermore, the filler−filler interaction is changed to $\varepsilon_{nn} = 6.0$. The snapshots for the aggregation process are shown in Figure 9a. In this process, the polymer−filler and filler−filler interaction energies are also monitored, as shown in Figure 9b. Obviously, after the time evolution $t = 2000\tau$, both polymer−filler and filler−filler interaction energies remain unchanged, suggesting the end of the aggregation process. Accordingly, the polymer−filler and filler−filler interaction energies can serve as an indicator to reflect the aggregation process. In the following section, the effect of the temperature on the aggregation process is studied. For simplicity, Figure 10a only shows the change of the polymer−filler interaction energies at three typical temperatures. The equilibrium time of the aggregation process t_e can therefore be well extracted from the change of the polymer−filler interaction energy, as evidenced in Figure 9b. Namely, the accurate equilibrium time corresponds to the occurrence of the plateau of the polymer−filler interaction

dx.doi.org/10.1021/la201073m |*Langmuir* 2011, 27, 7926–7933

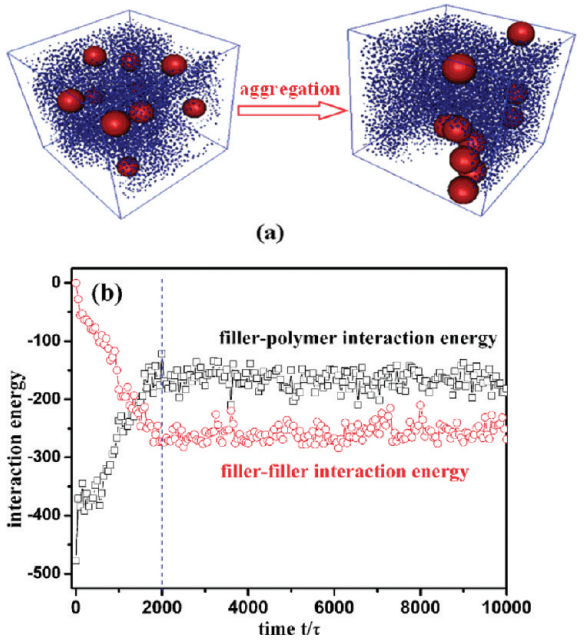

Figure 9. After deletion of the grafted polymer chains, the filler−filler interaction is changed from ε_{nn} = 1.0 to ε_{nn} = 6.0. (a) Snapshots of the aggregation process. (b) Change of the polymer−filler and filler−filler interactions as a function of time.

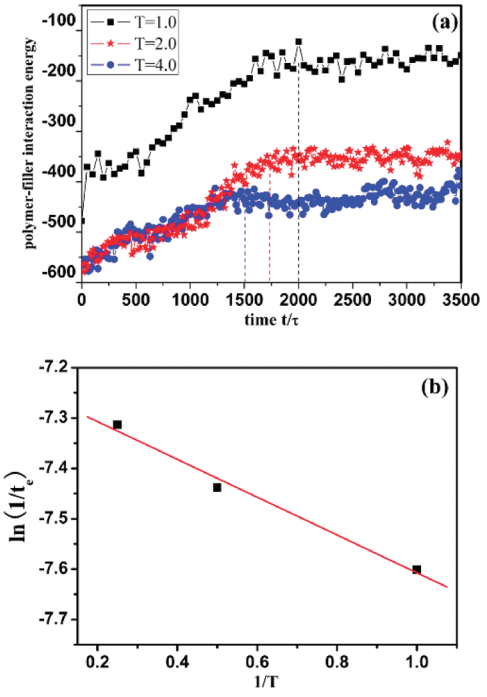

Figure 10. (a) Change of the polymer−filler interaction energy as a function of the aggregation time for different temperatures. The dotted lines represent the equilibrium time of the aggregation process. (b) Logarithm of the aggregation rate (the inverse of the aggregation equilibrium time t_e) as a function of the inverse of the temperature.

energy with respect to time. In Figure 10b, the inverse of t_e as a function of the inverse of the temperature is plotted, and an approximate linear relationship is obtained, suggesting that the

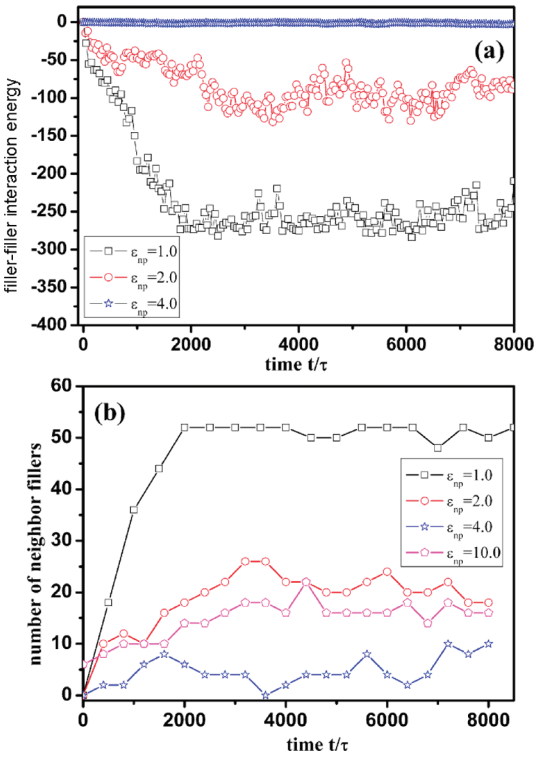

Figure 11. (a) Effect of different polymer−filler interactions on the filler aggregation process. (b) Change of the total number of neighbor fillers as a function of the aggregation process.

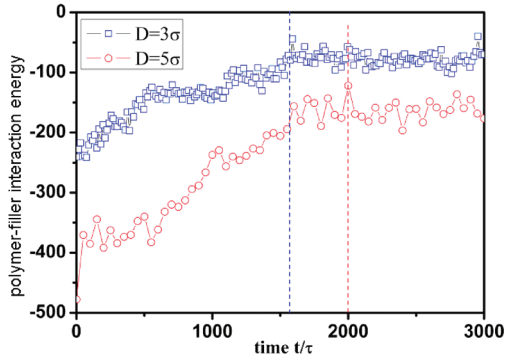

Figure 12. Change of the polymer−filler interaction during the aggregation process for different filler sizes. The dotted lines represent the equilibrium time of the aggregation process.

aggregation process exhibits an Arrhenius-like behavior, which implies that the rate of the filler aggregation is very sensitive to high temperature. According to this observation, we can rationalize that, for the glassy PNCs, the filler dispersion is not always good, since the dispersion of the NPs will easily reach equilibrium during the processing at high temperature (above the melting temperature) under an external force. Simultaneously, the aggregation rate of the NPs will become faster.

The polymer−filler interaction is also varied to examine its effects on the filler aggregation. As shown in Figure 11a, the aggregation extent decreases with an increase of the polymer−filler interaction. This is consistent with the experimental observation that the aggregation or coarsening rate can be decreased by adding the coupling agent in silica-filled rubber

dx.doi.org/10.1021/la201073m |*Langmuir* 2011, 27, 7926–7933

compounds,[22] which enhances the interfacial interaction. To quantitatively analyze the aggregation extent, the total number of neighbor particles around every particle is calculated within a distance of $L = 6.5\sigma$, as shown in Figure 11b. However, it is noted that, with a further increase of the polymer−filler interaction, such as $\varepsilon_{np} = 10.0$, the aggregation extent of the fillers increases, as indicated by the increased number of neighbor fillers, compared to $\varepsilon_{np} = 4.0$. This is consistent with the results displayed in Figure 1. Finally, the effects of the filler size on its aggregation are presented. As shown in Figure 12, the aggregation equilibrium time for the filler with its diameter $D = 3\sigma$ is approximately 1500τ, while 2000τ for the filler with its diameter $D = 5\sigma$, indicating that the fillers with smaller size aggregate more quickly, which can be rationalized by the Stokes−Einstein law.[34] With a larger diffusion coefficient, the smaller NPs exhibit a more rapid coarsening and thus require a shorter time to reach aggregation equilibrium.

4. CONCLUSIONS

Through a detailed coarse-grained MD simulation, we have mainly addressed the dispersion and aggregation mechanisms of NPs in PNCs at different loading levels. The results indicate that there exist three different states of filler spatial organization as a function of the polymer−filler interaction, which is in good agreement with the theoretical prediction from Schweizer et al. Furthermore, a good dispersion with large interparticle distance was obtained by grafting polymer chains on the filler surface. To mimick nanoparticle coarsening in experiments, we have investigated the effects of the temperature, polymer−filler interaction, and filler size on the aggregation process by cutting the grafted polymer chains. Generally, this further understanding of the filler dispersion and aggregation at the molecular level can assist in the rational design to achieve good nanoparticle dispersion and thus to obtain homogeneous PNCs for long-life service.

AUTHOR INFORMATION

Corresponding Author

*E-mail: caodp@mail.buct.edu.cn (D.C.); zhanglq@mail.buct.edu.cn (L.Z.); zhanhu.guo@lamar.edu (Z.G.).

ACKNOWLEDGMENT

This work was supported by the Outstanding Young Scientists Foundation of the National Natural Science Foundation (NSF) of China (Grant 50725310) the NSF of China (Grants 20776005, 20736002, and 20874005), The National High Technology Research and Development Program of China (863 Program) (Grant 2009AA03Z338), the National Basic Research Program (Grant 2011CB706900) and Novel Team (Grant IRT0807) from the Ministry of Education, and the "Chemical Grid Project" and Excellent Talents Funding of BUCT. Z.G. acknowledges support from the U.S. National Science Foundation (Nanoscale Interdisciplinary Research Team and Materials Processing and Manufacturing) under Grant CMMI 10-30755.

REFERENCES

(1) Paul, D. R.; Robeson, L. M. *Polymer* **2008**, *49*, 3187.
(2) Mackay, M. E.; Tuteja, A.; Duxbury, P. M.; Hawker, C. J.; Van Horn, B.; Guan, Z. B.; Chen, G. H.; Krishnan, R. S. *Science* **2006**, *311*, 1740.
(3) Tuteja, A.; Duxbury, P. M.; Mackay, M. E. *Phys. Rev. Lett.* **2008**, *100*, 077801.
(4) Pomposo, J. A.; de Luzuriaga, A. R.; Etxeberria, A.; Rodriguez, J. *Phys. Chem. Chem. Phys.* **2008**, *10*, 650.
(5) Krishnamoorti, R. *MRS Bull.* **2007**, *32*, 341.
(6) Khare, H. S.; Burris, D. L. *Polymer* **2010**, *51*, 719.
(7) Hooper, J. B.; Schweizer, K. S. *Macromolecules* **2005**, *38*, 8858.
(8) Ganesan, V.; Ellison, C. J.; Pryamitsyn, V. *Soft Matter* **2010**, *6*, 4010.
(9) Hall, L. M.; Jayaraman, A.; Schweizer, K. S. *Curr. Opin. Solid State Mater. Sci.* **2010**, *14*, 38.
(10) Starr, F. W.; Douglas, J. F.; Glotzer, S. C. *J. Chem. Phys.* **2003**, *119*, 1777.
(11) Fermeglia, M.; Pricl, S. Multiscale Molecular Modelling of Dispersion of Nanoparticles in Polymer Systems of Industrial Interest. *Iutam Symposium on Modelling Nanomaterials and Nanosystems*; Springer: Dordrecht, The Netherlands, 2009; Vol. 13, p 261.
(12) Lan, Q.; Francis, L. F.; Bates, F. S. *J. Polym. Sci., Part B: Polym. Phys.* **2007**, *45*, 2284.
(13) Wang, X. R.; Foltz, V. J.; Rackaitis, M.; Bohm, G. G. A. *Polymer* **2008**, *49*, 5683.
(14) Xu, C.; Ohno, K.; Ladmiral, V.; Composto, R. J. *Polymer* **2008**, *49*, 3568.
(15) Harton, S. E.; Kumar, S. K. *J. Polym. Sci., Part B, Polym. Phys.* **2008**, *46*, 351.
(16) Xu, J. J.; Qiu, F.; Zhang, H. D.; Yang, Y. L. *J. Polym. Sci., Part B, Polym. Phys.* **2006**, *44*, 2811.
(17) Smith, G. D.; Bedrov, D. *Langmuir* **2009**, *25*, 11239.
(18) Jayaraman, A.; Schweizer, K. S. *Macromolecules* **2008**, *41*, 9430.
(19) Jayaraman, A.; Schweizer, K. S. *Macromolecules* **2009**, *42*, 8423.
(20) Jayaraman, A.; Schweizer, K. S. *Mol. Simul.* **2009**, *35*, 835.
(21) Nair, N.; Jayaraman, A. *Macromolecules* **2010**, *43*, 8251.
(22) Mihara, S.; Datta, R. N.; Noordermeer, J. W. M. *Rubber Chem. Technol.* **2009**, *82*, 524.
(23) Bohm, G. G. A.; Nguyen, M. N. *J. Appl. Polym. Sci.* **1995**, *55*, 1041.
(24) Gerspacher, M.; Nikiel, L.; Yang, H. H.; O'Farrell, C. P.; Schwartz, G. A. *Kautsch. Gummi Kunstst.* **2002**, *55*, 596.
(25) Lin, C. J.; Hergenrother, W. L.; Alexanian, E.; Bohm, G. G. A. *Rubber Chem. Technol.* **2002**, *75*, 865.
(26) Lin, C. J.; Hogan, T. E.; Hergenrother, W. L. *Rubber Chem. Technol.* **2004**, *77*, 90.
(27) Bohm, G. A.; Tomaszewski, W.; Cole, W.; Hogan, T. *Polymer* **2010**, *51*, 2057.
(28) Kalra, V.; Escobedo, F.; Yong Lak, J. *J. Chem. Phys.* **2010**, *132*, 024901.
(29) Filippone, G.; Romeo, G.; Acierno, D. *Langmuir* **2010**, *26*, 2714.
(30) Jia, X. L.; Listak, J.; Witherspoon, V.; Kalu, E. E.; Yang, X. P.; Bockstaller, M. R. *Langmuir* **2010**, *26*, 12190.
(31) Kiel, J. W.; Eberle, A. P. R.; Mackay, M. E. *Phys. Rev. Lett.* **2010**, *105*, 168701.
(32) Meli, L.; Green, P. F. *ACS Nano* **2008**, *2*, 1305.
(33) Hooper, J. B.; Schweizer, K. S. *Macromolecules* **2006**, *39*, 5133.
(34) Liu, J.; Cao, D. P.; Zhang, L. Q. *J. Phys. Chem. C* **2008**, *112*, 6653.
(35) Smith, J. S.; Bedrov, D.; Smith, G. D. *Compos. Sci. Technol.* **2003**, *63*, 1599.
(36) Allen, M. P.; Tildesley, J. *Computer Simulation of Liquids*; Oxford University Press: Oxford, U.K., 1987.
(37) Desai, T.; Keblinski, P.; Kumar, S. K. *J. Chem. Phys.* **2005**, *122*, 134910.
(38) Plimpton, S. *J. Comput. Phys.* **1995**, *117*, 1.
(39) Liu, J.; Cao, D. P.; Zhang, L. Q.; Wang, W. C. *Macromolecules* **2009**, *42*, 2831.
(40) Goswami, M.; Sumpter, B. G. *J. Chem. Phys.* **2009**, *130*, 134910.